Available online at www.sciencedirect.com
ScienceDirect
Ceramics International 34 (2008) 631–638
CERAMICS INTERNATIONAL
www.elsevier.com/locate/ceramint

Synthesis and microstructure of the Ti_3SiC_2 in SiC matrix grown by chemical vapor deposition

Tien-Chai Lin [a,*], Min-Hsiung Hon [b]

[a] Department of Electrical Engineering, Kun Shan University, Tainan, Taiwan, ROC
[b] Department of Materials Science and Engineering, National Chen Kung University, Tainan, Taiwan, ROC

Received 30 March 2006; received in revised form 8 May 2006; accepted 10 January 2007
Available online 13 March 2007

Abstract

Ti_3SiC_2 + SiC and TiC + SiC were deposited on graphite substrate at 1300–1600 °C by chemical vapor deposition with $TiCl_4$, $SiCl_4$, C_3H_8, H_2 as reactive gases. Process parameters such as temperature, pressure, concentration of C_3H_8 were varied to study their effects on the phases and microstructure of the deposited layers. The results show that binary phases of Ti_3SiC_2 + SiC are formed at temperature less than 1400 °C. For temperature above 1500 °C, TiC + SiC phases are formed. Increase of the process pressure causes the disappearance of Ti_3SiC_2 and the formation of TiC. The surface morphology of Ti_3SiC_2 shows a plate-like structure. The hardness of Ti_3SiC_2 + SiC and TiC + SiC is HV4251 and HV4612 respectively for a load of 10 g.

Keywords: B. Composites; C. Hardness; D. Carbides; Chemical vapor deposition

1. Introduction

In the last decade, lots of efforts have been made on the study of multiphase composite ceramics [1–5]. Those studies were primary conducted with conventional sintering process at high temperature and high pressure. Multiphase composite ceramics can improve the deficiency of low toughness of hard ceramics materials. The most attractive matrix of composite materials at present is SiC for its high strength, good creep resistance and high temperature oxidation resistance; therefore, SiC is a very promising material for the application in the mechanical industries. However, its potential application is limited by its low fracture toughness. Adding second phase to SiC matrix resists crack propagation. It has been proven as an effective way to improve fracture toughness. For instance, Si_3N_4, TiB_2, B_4C, BN, AlN, MoS_2 were added to improve the fracture toughness, electrical properties and oxidation resistance of SiC.

Ternary compound Ti_3SiC_2 [6–10] possesses characters of ceramics such as high melting point, high oxidation resistance, thermal shock resistance and characters of plastic-like materials with low hardness as well. TiO_2 and SiO_2 are easy to be formed on the surface of Ti_3SiC_2, which make Ti_3SiC_2 have a better oxidation resistance than BN and graphite and become a very promising new soft ceramics material.

Structural ceramics with uniform distribution of second phase, controlled grain size, free of impurity on the grain boundary and multi-component constitution can be prepared by chemical vapor deposition (CVD) process [11–14]. The purpose of this study is to prepare a uniformly distributed Ti_3SiC_2 dispersion phase on SiC matrix by CVD process and to investigate the formation of phases and microstructures.

2. Experimental procedure

The deposits were prepared with a cold-wall CVD reactor shown as Fig. 1. Graphite with an effective dimension of 40 mm × 12 mm × 2 mm was served as the substrate and the heater as well. An infrared pyrometer was used for temperature monitoring. The venting system was composed of a set of pump, and pressure control valves were used to control the pressure inside the reactor. Because the vented waste gases contain chloride acid, a NaOH tower was installed for neutralization purpose. H_2, C_3H_8, $TiCl_4$ and $SiCl_4$ were chosen as the reactive materials. Carbon source used C_3H_8 instead of

* Corresponding author. Tel.: +886 6 2050518; fax: +886 6 2050298.
E-mail address: tienchai@mail.ksu.edu.tw (T.-C. Lin).

0272-8842/$34.00
doi:10.1016/j.ceramint.2007.01.005

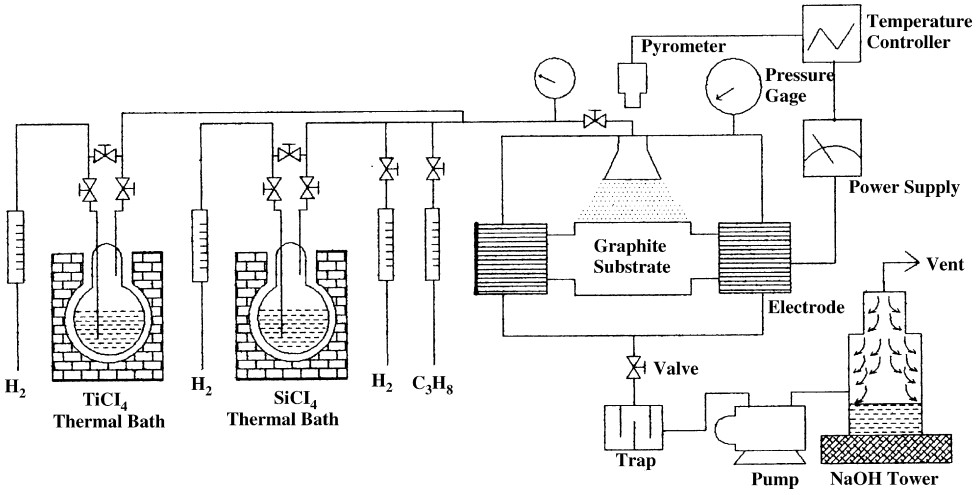

Fig. 1. Schematic illustration of CVD Si–Ti–C deposition system.

CH_4, due C_3H_8 contains more carbon to hydrogen ration than CH_4 source. $TiCl_4$ and $SiCl_4$ were liquids which used H_2 as a carrier gas to feed into a thermostat of $TiCl_4$ and $SiCl_4$. Then, the saturated vapor was carried into the reactor. The flow rate of hydrogen carrier gas is controlled by ball flow meter. And then the flow rate of $TiCl_4$ and $SiCl_4$ are calculated by the equation given as follows.

$$V_1 = \frac{P_1}{760 - P_1} V_{H_2} \quad (1)$$

Where V_1 is the flow rate of $TiCl_4$ or $SiCl_4$. V_{H_2} is the flow rate of H_2 which feed into the thermostat. P_1 is the saturated vapor pressure of $TiCl_4$ or $SiCl_4$ at setting temperature. Three ball flow meter was used in our experiment to directly read out H_2 flow rate, one for main gas and others for carrier gases, and then to calculate the flow rate of $TiCl_4$ and $SiCl_4$ by this equation. Table 1 shows the process parameters in detail. In our experiment, the deposition time is constant of 30 min. The typical deposition rate is 20 μm/min at growth parameters of 1500 °C, 100 torr, C_3H_8 = 25 sccm, $TiCl_4/(TiCl_4 + SiCl_4)$ = 0.65 and H_2 = 3000sccm.

The structures of deposits were analyzed with X-ray diffraction (XRD). A scanning electron microscope (SEM) was used to observe the surface morphologies of deposits. Specimens for plain view and cross section view observations were prepared by cutting, mounting, grinding and polishing procedures. An optical microscope was used for the observation of general features of the microstructure. Transmission electron microscopy (TEM) was used to investigate the structure of Ti_3SiC_2 phase in SiC matrix.

Table 1
Lists of experimental parameters

Parameters	Value
Deposition temperature	1300–1600 °C
Process pressure	40–300 torr
Deposition time	30 min
Flow rate	
H_2	2500 sccm
$TiCl_4$	82 sccm
$SiCl_4$	45 sccm
C_3H_8	25–35 sccm

The mechanical property of deposits was evaluated with Vickers micro-hardness measurement. The relationship between hardness and loads was investigated on varying applied loads for hardness measurements using a polished specimen.

3. Results and discussion

3.1. Si–Ti–C system deposits

$SiCl_4$, $TiCl_4$ and C_3H_8 were used as the reactive gases sources of Si, Ti and C. In the CVD reaction, there are several phases deposited on graphite substrates. The constitution of phases can be well controlled by varying pressure and temperature at a fixed flow rate of reactive gases. Fig. 2 shows XRD analysis of Si–Ti–C system growth on different temperatures at fixed $TiCl_4$ = 82 sccm, $SiCl_4$ = 45 sccm, and C_3H_8 = 25 sccm. The phases of SiC, TiC and Ti_3SiC_2 were identified as the dominant phases in the film. Referring to JCPDS cards, SiC which is ZnS structure with a lattice constant of a_{SiC} = 0.4358 nm is identified. TiC which is the NaCl structure with a lattice constant of a_{TiC} = 0.4327 nm is identified. According to Goto and Hirai report [15], the structure of Ti_3SiC_2 is hexagonal of D6h4-D63/mmc with a lattice constant of $a_{Ti_3SiC_2} = 0.3064$nm, $c_{Ti_3SiC_2} = 1.7650$nm and a theoretical density of 4.531 g/cm^3. SiC and Ti_3SiC_2 are dominant phases at 1300 °C. The peaks of XRD patterns are identified in which the (1 1 1), (2 2 0), (3 1 1) are for SiC and the $(1\,0\,\bar{1}\,0), (1\,0\,\bar{1}\,4), (1\,0\,\bar{1}\,5), (1\,1\,\bar{2}\,0)$ are for Ti_3SiC_2. The appearing phases at 1400 °C are the same with those at 1300 °C. When the temperature is increased to 1500 °C, Ti_3SiC_2 phase will disappear, and TiC and SiC phases appear in the deposits. Since both of TiC and SiC are cubic structure and with very close values of lattice constants, it is hard to distinguish between SiC and TiC phases under the influence of a thermal stress induced by cooling process in high temperature

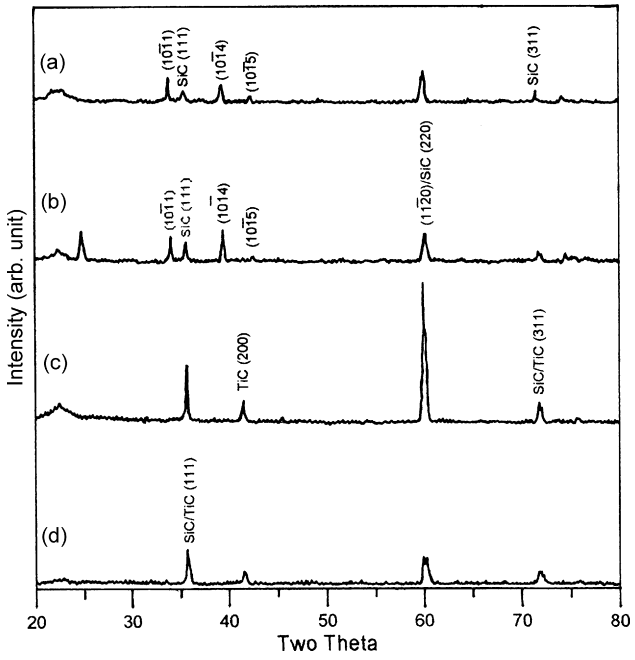

Fig. 2. The XRD analysis of the Si–Ti–C system deposits at different reaction temperatures: (a) 1300 °C, (b) 1400 °C,(c) 1500 °C, (d) 1600 °C; 100 torr; C_3H_8 = 25 sccm, TiC_4 = 82 sccm, $TiCl_4/(TiCl_4 + SiCl_4)$ = 0.65 and H_2 = 2500 sccm.

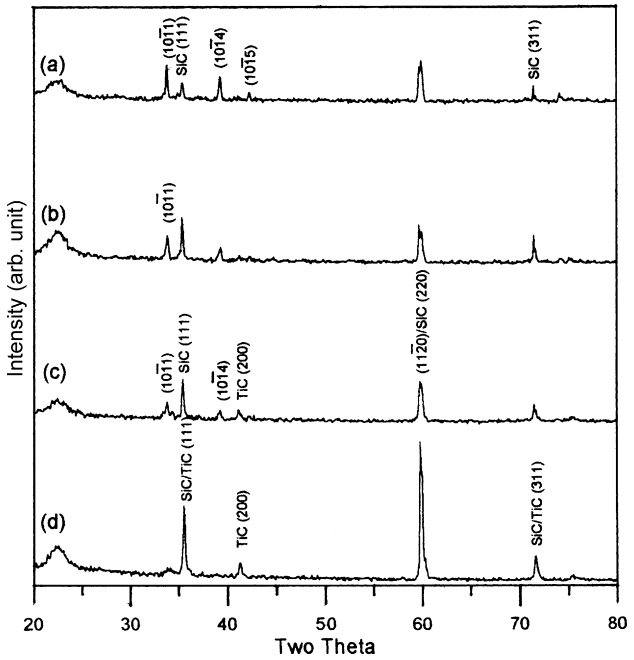

Fig. 3. The XRD analysis of the Si–Ti–C system deposits at different total reactive pressure: (a) 40 torr, (b) 100 torr, (c) 200 torr, (d) 300 torr; 1300 °C; C_3H_8 = 25 sccm, TiC_4 = 82 sccm, $TiCl_4/(TiCl_4 + SiCl_4)$ = 0.65 and H_2 = 2500 sccm.

CVD. When we studied the pure β-SiC grown by CVD at 1500 °C, the XRD results showed that (1 1 1), (2 2 0) and (3 1 1) were found but without (2 0 0) peak. In the Si–Ti–C system, diffraction peak of (2 0 0) appeared for deposits of 1500 °C. Hence, we reasonably suggest that (2 0 0) peak is caused by the presence of CVD TiC phase in the deposits to form a SiC/TiC composite. The preferred orientation for the deposits of 1500 °C is (2 2 0) with a narrow half-maximum line breadth. The structure of the deposits at 1600 °C is the same with that of 1500 °C which is composed of SiC and TiC.

Fig. 3 shows the results of XRD analysis for deposits obtained with totally different pressure process. At pressure of 40 and 100 torr (1 mtorr = 0.1333 pa), Ti_3SiC_2 and SiC are the dominate phases. With an increasing total pressure to 200 torr, the formation of a mixture phase of TiC, SiC and Ti_3SiC_2 are identified. Ti_3SiC_2 phase almost disappeared at pressure of 300 torr and only a two-phase of SiC + TiC existed. Racault et al. [16,17] have performed an analysis of thermodynamics for the CVD $TiCl_4$–$SiCl_4$–CH_4 system at 1000 °C and 2–50 kPa. They made a conclusion that no Ti_3SiC_2 will be formed at 50 kPa and pure Ti_3SiC_2 phase will be obtained at low pressure. When the pressure increases above 20 kPa, Ti_3SiC_2 + TiC phase or Ti_3SiC_2 + TiC + SiC phase will be obtained. The relative amount of Ti_3SiC_2 will be reduced with a function of increasing pressure.

In the system of $TiCl_4$, $SiCl_4$, C_3H_8 and H_2, the structure analysis by XRD obtained with changing C_3H_8 concentration from 25 to 35 sccm is shown in Fig. 4. SiC + Ti_3SiC_2 phases are dominate at C_3H_8 = 25 sccm. When C_3H_8 concentration increases to 35 sccm, the SiC + TiC phase is dominated in the deposit. The carbon concentration increases in boundary layer on substrate surface when the C_3H_8 concentration rises in reaction chamber. The structure will be changed from SiC + Ti_3SiC_2 to SiC + TiC for rich carbon equilibrium phase.

Fig. 5 shows the CVD phase map of the Si–Ti–C system according to the XRD phase analysis. The map is composed of

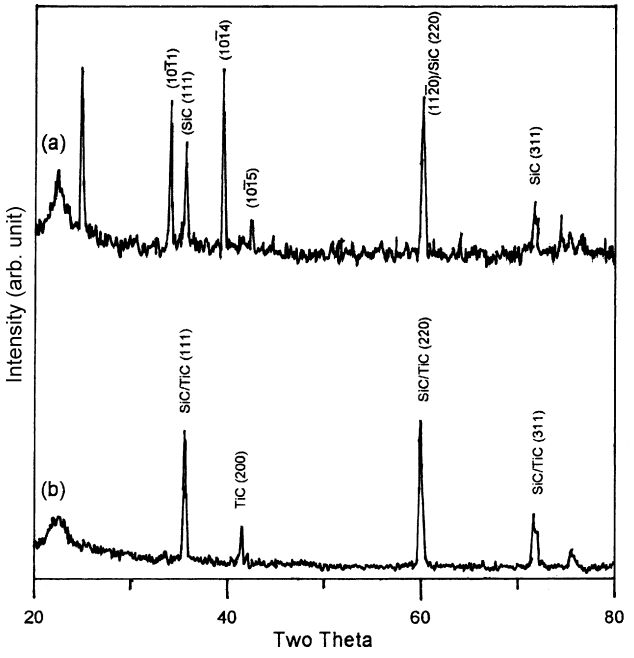

Fig. 4. The XRD analysis of the Si–Ti–C system deposits at different C_3H_8 concentrations: (a)25 sccm, (b) 35 sccm; 1400 °C; 100 torr;TiC_4 = 82sccm, $TiCl_4/(TiCl_4 + SiCl_4)$ = 0.65 and H_2 = 2500 sccm.

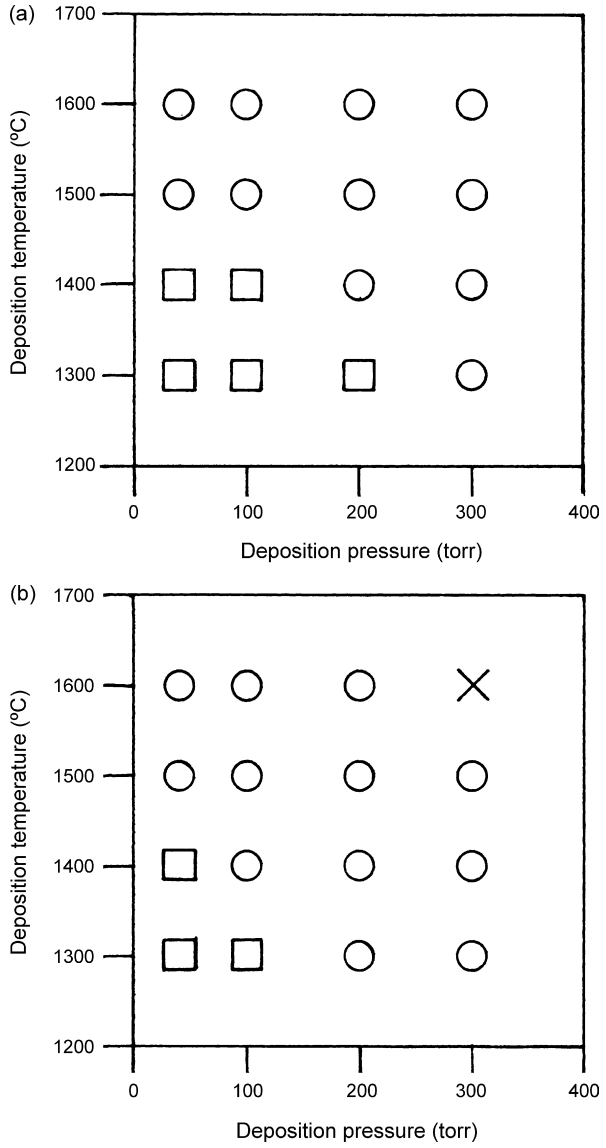

Fig. 5. The CVD phase map of Si–Ti–C system: (a) $C_3H_8 = 25$ sccm; (b) $C_3H_8 = 35$ sccm; (□) Ti3SiC2 + SiC; (○) SiC + TiC; (×) no-deposit.

three regions corresponding to different temperatures and pressure which are Ti_3SiC_2 + SiC, SiC + TiC and no-deposit. According to Fig. 5(a) at $C_3H_8 = 25$ sccm, the phase of Ti_3SiC_2 + SiC is found at low temperature and low pressure region respective to the phase of SiC + TiC. Ti_3SiC_2 begins to appear at 1300 °C and in pressure of 40, 100 or 200 torr. When the temperature is kept at 1400 °C, Ti_3SiC_2 is obtained only at pressure of 40 or 100 torr. The results shows the region of Ti_3SiC_2 shrinks in pressure depend on the temperature increasing. The SiC + TiC region is expanded at 1400 °C which indicates the SiC + TiC is a more stable phase in higher temperature. In Fig. 5(b) at $C_3H_8 = 35$ sccm, Ti_3SiC_2 can be formed at 1300 °C and 1400 °C in pressure region of 40 and 100 torr. Comparing to Fig. 5(a) at $C_3H_8 = 25$ sccm, the depositing region of Ti_3SiC_2 is shrunk. It indicates that increasing the C_3H_8 concentration is unfavorable for the growth of Ti_3SiC_2 and favorable for SiC + TiC. No deposit region, which means without any deposit on substrates, is found at 1600 °C at 300 torr and $C_3H_8 = 35$ sccm. This phenomenon is due to a homogeneous nucleation appeared in vapor phase at such high temperature and high C_3H_8 concentration.

3.2. Microstructure

Surface morphologies of the deposits at various temperatures are shown in Fig. 6. At 1300 °C, the deposit shows a plate-like structure which is corresponding to Ti_3SiC_2. The plates have a growth direction perpendicular to the substrate. Some small particles with a shape of polyhedral cones can be found between the plates. At 1400 °C, plate-like structures of Ti_3SiC_2 are still there. A large amount of small particles with polyhedral cones appeared to cover all around of the Ti_3SiC_2 plates. Ti_3SiC_2 with plate-like structure disappeared at 1500 °C, which agrees with X-ray analysis results. It indicates no Ti_3SiC_2 existed. The deposit surface is covered with large particles of non-polyhedral shape. The large particle is also covered with tiny particles on surface. When temperature increases to 1600 °C, a facet morphology becomes clear in the deposit. A sufficient thermal energy is supplied to atoms at high temperature. Atoms actively diffuse into a favorite site for reducing total energy. A planar surface with low energy is formed, that is favors polyhedral cone formation.

As indicated in Fig. 3 for total pressure increasing from 40 to 300 torr, the phases of deposits will be changed from Ti_3SiC_2 + SiC to SiC + TiC. Fig. 7 shows the transition of morphologies observed by SEM. For deposits at 40–200 torr,all of the morphologies are plate-like structures which are mainly composed of Ti_3SiC_2. For the deposit at 300 torr, a facet is obtained indicating that the deposit is mainly composed of SiC + TiC.

Fig. 8 shows a top view of the deposit observed by an optical microscope previous to polished specimen. Fig. 8(a) is for temperature of 1400 °C and Fig. 8(b) is for 1500 °C. XRD analysis shows that Ti_3SiC_2 + SiC are the dominate phases for 1400 °C. SiC + TiC are the dominate phases for 1500 °C. The regions of white color in Fig. 8(a) and (b) are Ti_3SiC_2 and TiC, respectively, since both of them are more reflective to light than SiC. As indicated in the figures, the particle size of Ti_3SiC_2 is larger than that of TiC. A cross sectional view of the deposit at 1400 °C is shown in Fig. 9. A region with white color is the structure of Ti_3SiC_2 and one with grey color is SiC. From the microstructures known, the deposits are columnar structures.

Fig. 10 shows the composition mapping of cross section with Ti_3SiC_2 + SiC phases by WDS analysis. For the elements of Ti, Si and C analysis, since white region is Ti_3SiC_2 and grey region is SiC, therefore the results show that the content of silicon is higher in grey region and lower in white region. From the point of view in atomic percentage, there are 50 at% of Si in SiC but only 17 at% in Ti_3SiC_2. To the contrary, element Ti shows a higher value in white region and a lower value in grey region. The distribution of C mapping is similar to that of Si.

Fig. 11 shows the microstructure of Ti_3SiC_2 + SiC binary phase structure observed by TEM. Fig. 11(a) shows the dark

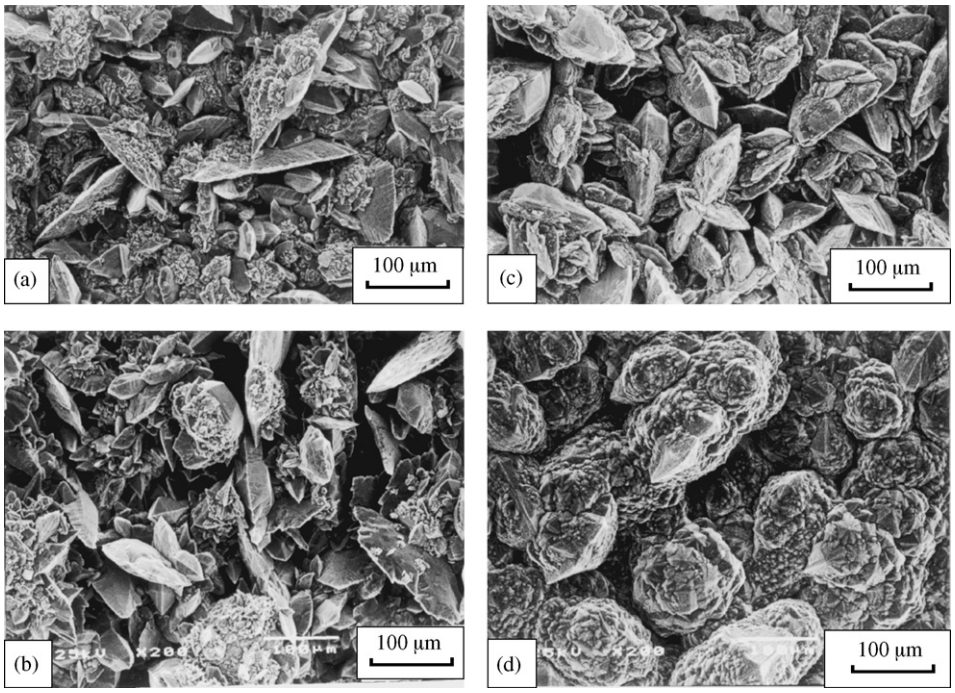

Fig. 6. Surface morphologies of the deposits of various deposition temperature observed by SEM: (a) 1300 °C, (b) 1400 °C, (c) 1500 °C, (d) 1600 °C, 1300 °C; 100 torr; C_3H_8 = 25 sccm, TiC_4 = 82 sccm, $TiCl_4/(TiCl_4 + SiCl_4)$ = 0.65 and H_2 = 2500sccm.

field image. The schematic illustration for the distribution of Ti_3SiC_2 and SiC is shown in Fig. 11(b). Some stacking faults are observed in the grain of Ti_3SiC_2. Stacking fault with micro-twin is found in grain B. The Ti_3SiC_2 phase is surrounded by SiC phase. Diffraction pattern of grain A and B are shown in Fig. 11(c) and (d). The orientation of $[\bar{2}\,1\,1\,0]$is identified to be the zone axis [18]. A 70.5° mutual–rotate relationship for these two patterns can be observed which is the twin angle for the <1 1 1> direction of FCC structure.

3.3. Hardness measurements

The mechanical properties of deposits are closely related to the phase constitution and microstructure of the deposits.

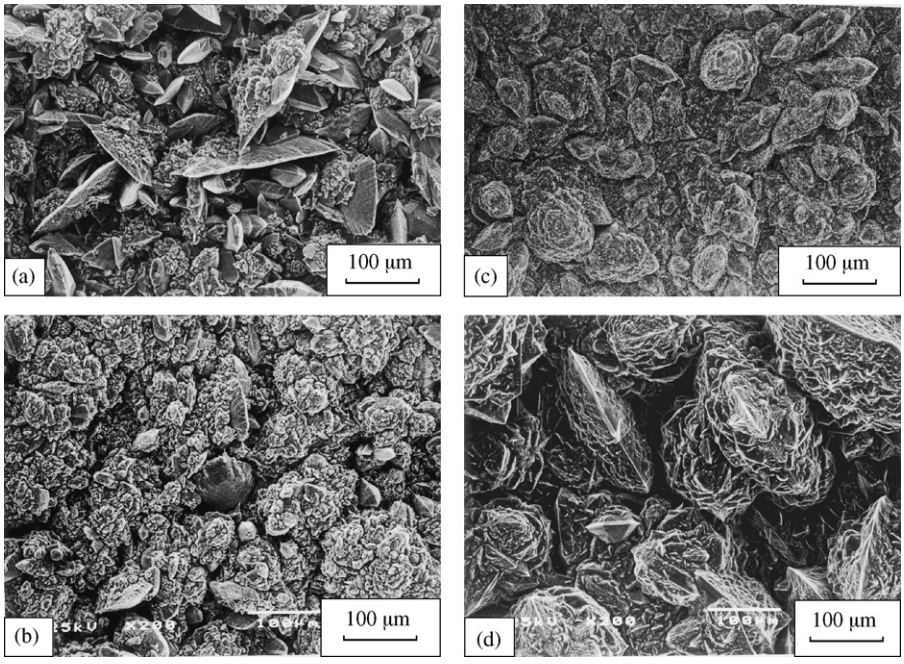

Fig. 7. Surface morphologies of the deposits of various deposition pressure observed by SEM: (a) 40 torr, (b) 100 torr, (c) 200 torr, (d) 300 torr; 1300 °C; C_3H_8 = 25 sccm, TiC_4 = 82 sccm, $TiCl_4/(TiCl_4 + SiCl_4)$ = 0.65 and H_2 = 2500 sccm.

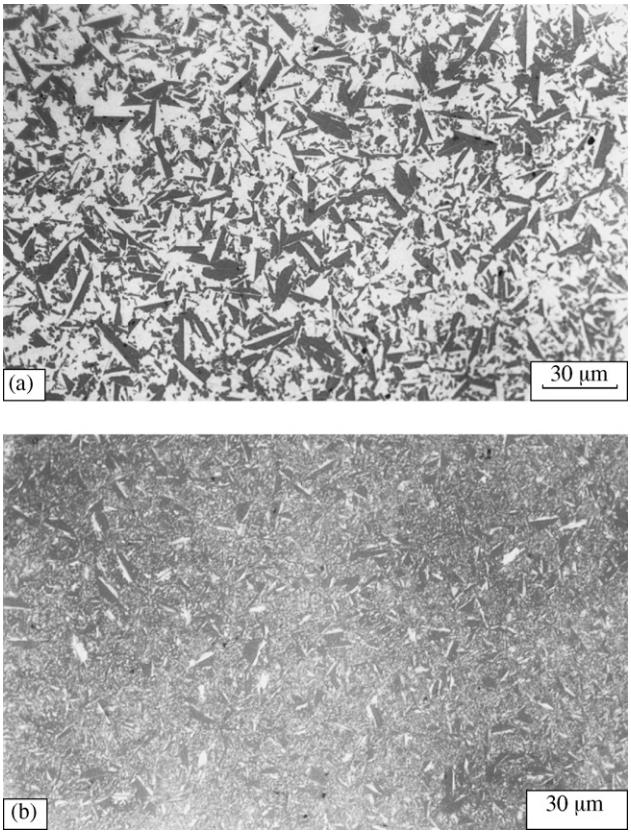

Fig. 8. The top view of polished deposits observed by optical microscopy: (a) 1400 °C, (b) 1500 °C; 100 torr; C_3H_8 = 25 sccm, TiC_4 = 82 sccm, $TiCl_4/(TiCl_4 + SiCl_4)$ = 0.65 and H_2 = 2500 sccm.

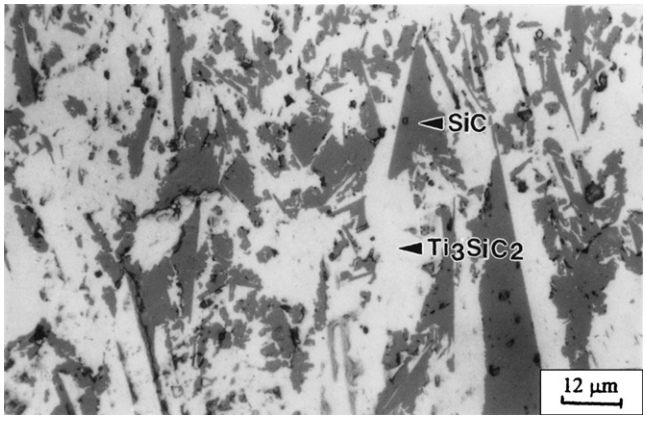

Fig. 9. The typical cross sectional view of Ti_3SiC_2 + SiC deposited at 1400 °C, 40 torr, C_3H_8 = 25 sccm, TiC_4 = 82sccm, $TiCl_4/(TiCl_4 + SiCl_4)$ = 0.65 and H_2 = 2500sccm observed by optical microscope.

Fig. 12 shows the results of the hardness measurements for CVD of Si–Ti–C system. The hardness of deposits decreases with the increase of applied load for measurements. Hardness of the specimen at 1600 °C reaches HV 4612 with a 10 g load, and reaches HV 2185 with a 200 g load. Hardness of the specimen at 1300 °C is HV 4215 for a 10 g load, and HV 1678 for a 200 g load which are lower than those at 1600 °C. This is mainly because the dominant structures are TiC + SiC phases for the deposits at 1600 °C and Ti_3SiC_2 for the deposits at 1400 °C, respectively, as the hardness of TiC is higher than that of Ti_3SiC_2. The hardness of Ti_3SiC_2 and SiC with larger grain size measured with a load of 10 g is HV 1580 and HV 4960,

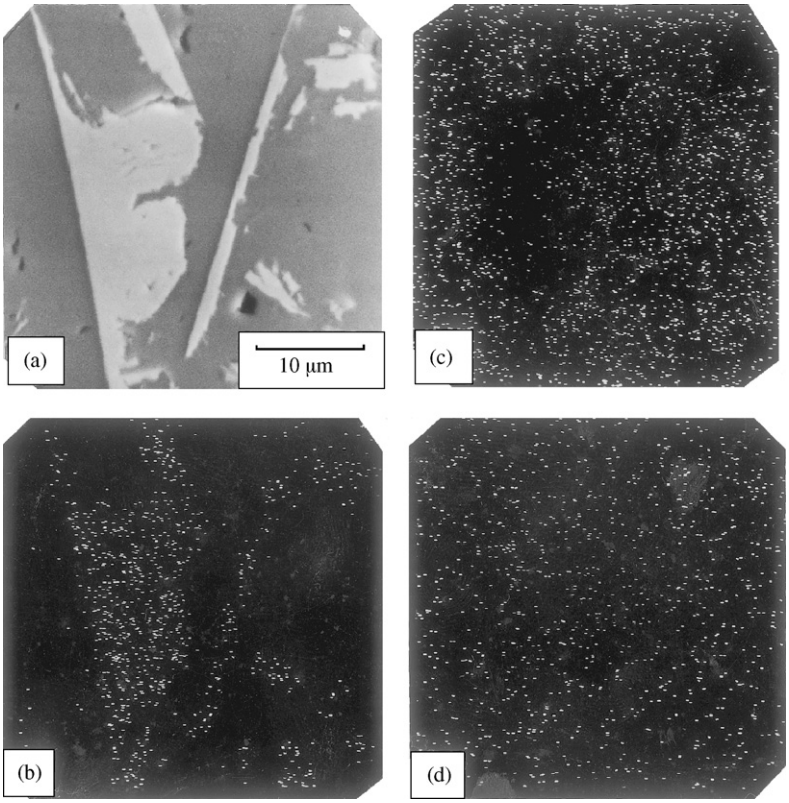

Fig. 10. Composition mapping analysis by WDS for the cross section of the deposits with Ti_3SiC_2 + SiC phases. (a) SEM image. (b) Ti mapping. (c) Si mapping. (d) C mapping.

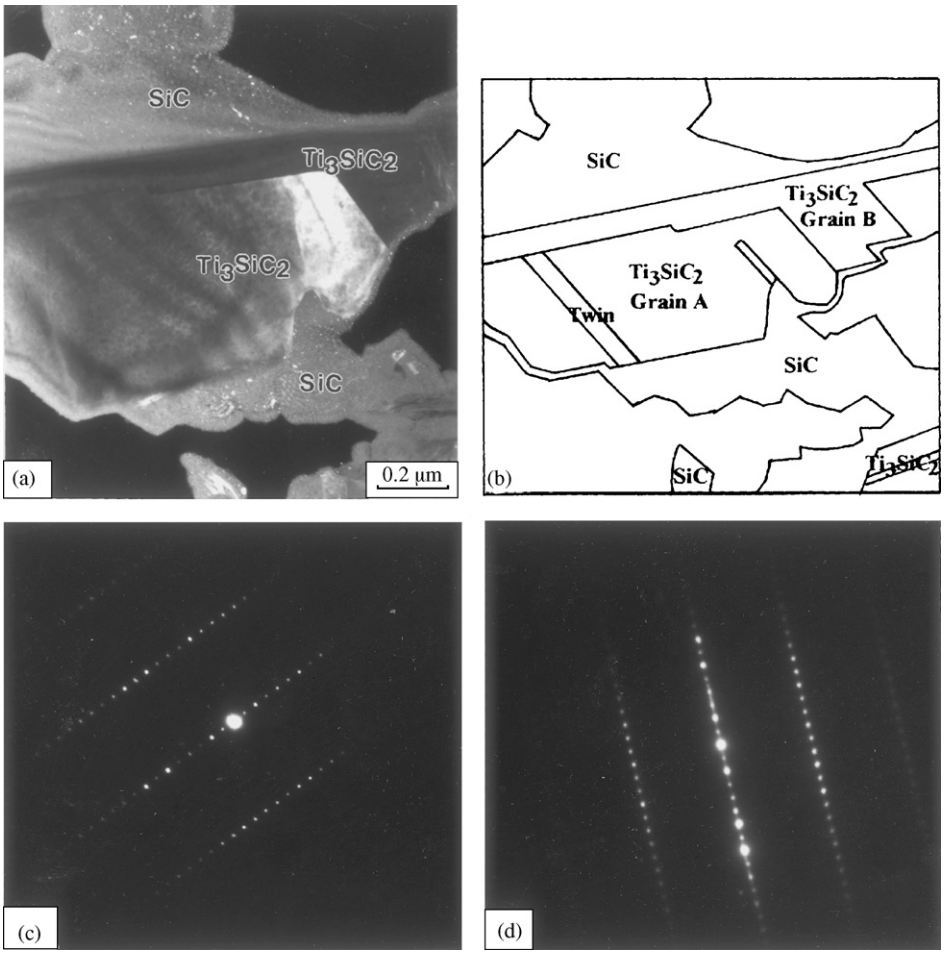

Fig. 11. Microstructure of Ti_3SiC_2 + SiC binary phase structure observed by TEM: (a) dark field image; (b) schematic illustration for the distribution of Ti_3SiC_2, and SiC; (c) a diffraction pattern of grain A; and (d) a diffraction pattern of grain B.

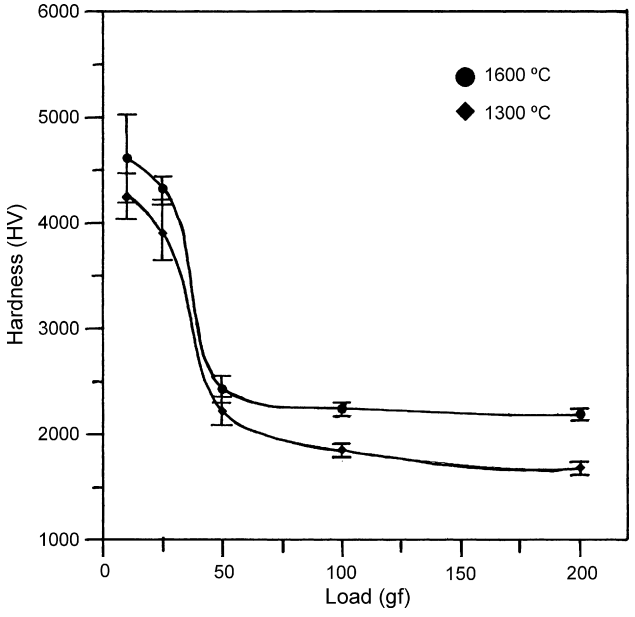

Fig. 12. Hardness measurements for CVD Si–Ti–C deposits grown at 100 torr, C_3H_8 = 25 sccm, TiC_4 = 82 sccm, $TiCl_4/(TiCl_4 + SiCl_4)$ = 0.65 and H_2 = 2500 sccm.

respectively, which indicates that the hardness of Ti_3SiC_2 is much less than that of SiC.

4. Conclusion

Ternary compound of Ti_3SiC_2 in SiC matrix can be successfully deposited by controlling the experimental parameters of CVD. Ti_3SiC_2 + SiC are formed at 1300 °C and 1400 °C. For temperature above 1500 °C, TiC + SiC are formed. The variation of pressure also affects the formation regions of various phases. With low pressure, Ti_3SiC_2 is facilitated to be formed. With high pressure, TiC is facilitated to be formed. The increase of C_3H_8 concentration will cause the disappearance of Ti_3SiC_2 phase and let the appearance of TiC + SiC. The surface morphology of Ti_3SiC_2 is a plate-like structure. The facet structures of TiC + SiC which were obtained at high temperature are well defined. The deposits are mainly grown as columnar structure. $[\bar{2}\,1\,1\,0]$ is found to be the zone axis of Ti_3SiC_2 by TEM analysis. Defects of twin and stacking fault are observed in the matrix. The angle between two Ti_3SiC_2 grains is 70.5°. The hardness of Ti_3SiC_2 + SiC and TiC + SiC is HV 4251 and HV 4612 for a load of 10 g, respectively. For a load of 200 g, the hardness of Ti_3SiC_2 + SiC and TiC + SiC is HV 1678 and HV2185, respectively.

Reference

[1] N.P. Padture, In situ-toughness silicon carbide, J. Am. Ceram. Soc. 77 (2) (1994) 519–523.

[2] R. Lundberg, L. Kahlman, R. Pompe, R. Carlsson, R. Warren, SiC-Whisker-Reinforced Si3N4 Compositesb, Am. Ceram. Soc. Bull. 66 (2) (1987) 330–333.

[3] S.T. Buljan, J.G. Baldoni, M.L. Huckabee, Si_3N_4–SiC Composites, Am. Ceram. Soc. Bull. 66 (2) (1987) 347–352.

[4] D. Baril, S.P. Tremblay, M. Fiset, Silicon carbide platelet-reinforced silicon nitride compositesb, J. Mat. Sci. 28 (1993) 5486–5494.

[5] J. XinXiang, R. Taylor, Dispersion of SiC wiskers in SiC whisker reinforced Si_3N_4 composite and related microstructural characteristics, Br. Ceram. Trans. 93 (1) (1994) 11–15.

[6] S. Arunajatesan, A.H. Carin, Synthesis of titanium silicon carbide, J. Am. Ceram. Soc. 78 (3) (1995) 667–672.

[7] L. Lis, R. Pampuch, J. Piekarczyk, L. Stobierski, Ceram. Int. 19 (1993) 219–222.

[8] K. Tang, C. Wang, X. Xu, Y. Huang, A study on power X-ray diffraction of Ti_3SiC_2, Mater. Lett. 55 (2002) 50–54.

[9] L. Yongming, P. Wei, L. Shuqin, C. Jian, W. Ruigang, L. Jianqiang, Synthesis of high-purity Ti3SiC2 polycrystals by hot-pressing of the elemental powers, Mater. Lett. 52 (2002) 245–247.

[10] R. Radhakrishnan, J.J. Williams, M. Akinc, Synthesis and high-temperature stability of Ti_3SiC_2, J. Alloys .Compd. 285 (1999) 85–88.

[11] W.Y. Lee, W.J. Lackey, P.K. Agrawal, G.B. Freeman, Simultaneous chemical vapor deposition of boron nitride and aluminum nitride, J. Am. Soc. 74 (10) (1991) 2649–2658.

[12] W.Y. Lee, W.J. Lackey, G.B. Freeman, P.K. Agrawal, D.J. Twait, Preparation of dispersed phase ceramic boron nitride and aluminum nitride composite coatings by chemical vapor deposition, J. Am. Ceram. Soc. 74 (9) (1991) 2134–2140.

[13] M. Touanen, F. Teyssandier, M.D.M. Maline, R. Hillel, J.L. Derep, Microcomposite and nanocomposite structures from chemical vapor deposition in the silicon-titanium-carbide system, J. Am. Ceram. Soc. 76 (6) (1993) 1473–1481.

[14] C. Kawai, J. Teraki, T. Hirano, T. Nomura, Fabrication of a functionally gradient material of TiC–SiC system by chemical vapor deposition, J. Ceram. Soc. Jap. 100 (9) (1992) 1117–1121.

[15] T. Goto, T. Hirai, Chemical vapor deposited Ti_3SiC_2, Mat. Res. Bull. 22 (1987) 1195–1201.

[16] C. Racault, F. Langlais, C. Bernard, On the chemical vapor deposition of Ti_3SiC_2 from $TiCl_4$-$SiCl_4$-CH_4-H_2 gas mixtures. Part I.A thermodynamic approach, J. Mat. Sci. 29 (1994) 5023–5040.

[17] C. Racault, F. Langlais, R. Naslain, Y. Kihin, On the chemical vapor deposition of Ti_3SiC_2 from $TiCl_4$- $SiCl_4$- CH_4- H_2 gas mixtures. Part II. An experimental approach, J. Mat. Sci. 29 (1994) 3941–3948.

[18] S. Arunajatesan, A.H. Carim, Symmetry and crystal structure of $Ti_3SiC_{2''}$, Mater. Lett. 20 (1994) 319–324.